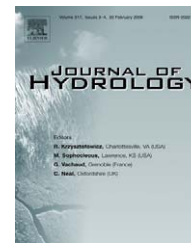




available at [www.sciencedirect.com](http://www.sciencedirect.com)



journal homepage: [www.elsevier.com/locate/jhydrol](http://www.elsevier.com/locate/jhydrol)



# Assessing stream–aquifer interactions through inverse modeling of flow routing <sup>☆</sup>

Jozsef Szilagyi <sup>a,c,\*</sup>, Marc B. Parlange <sup>b</sup>, Gabor Balint <sup>c</sup>

<sup>a</sup> School of Natural Resources, Conservation and Survey Division, University of Nebraska-Lincoln, 113 Nebraska Hall, Lincoln, NE 68588, USA

<sup>b</sup> Ecole Polytechnique Federale de Lausanne, Lausanne, Switzerland

<sup>c</sup> National Hydrological Forecasting Service, VITUKI, Hungary

Received 16 March 2005; received in revised form 3 November 2005; accepted 3 November 2005

## KEYWORDS

Stream–aquifer interactions;  
Baseflow separation;  
Flow routing;  
Inverse modeling

**Summary** Flux-exchange between stream and aquifer is assessed on a 85.9 km stretch of the Danube River in Hungary. Streamflow is modeled with a spatially and temporally discretized version of the linear kinematic wave equation written in a state-space form which allows for an easy inversion of flow routing. By knowing in- and outflow of the reach, lateral flux exchange between stream and groundwater can be assessed. Continuous baseflow separation, in terms of groundwater gained by the river between the two gaging stations, is made possible at the downstream station by routing groundwater discharged to the stream reach, separately from streamflow measured at the upstream gaging station.

© 2005 Elsevier B.V. All rights reserved.

## Introduction

Gaining insight into the dynamics of water fluxes exchanged between a stream and adjacent aquifer is not only scientifically challenging and, as such, worth pursuing for its own sake, but also has many practical implications. Groundwater contribution to the stream, especially, but not exclusively, during low-flow conditions, affects various water manage-

ment areas such as: irrigation design and scheduling in agriculture, water supply distribution and planning for urban areas, waste water dilution, river navigation, wildlife protection, as well as hydro- and nuclear power generation (providing cooling water to the plant), just to name a few. Streamflow behavior during baseflow conditions, i.e. when the flow in the stream is almost entirely maintained by groundwater, provides crucial information for aquifer characterization (Brutsaert and Nieber, 1977; Troch et al., 1993; Brutsaert and Lopez, 1998; Szilagyi et al., 1998; Parlange et al., 2001; Szilagyi, 2003a). Knowledge of this interaction between streamflow and groundwater during flood events can even significantly improve flood forecasting accuracy (Szilagyi, 2004a).

<sup>☆</sup> A contribution of the University of Nebraska Agricultural Research Division, Lincoln, NE 68583, USA. Journal Series No. 14998.

\* Corresponding author.

E-mail address: [jszilagy1@unl.edu](mailto:jszilagy1@unl.edu) (J. Szilagyi).

The importance of this interaction is reflected in the large number of publications on the subject within the hydrological, civil engineering, and hydrogeological literature, as was revealed by Tallaksen (1995). In practical applications, one of the most frequently looked for piece of information is the percentage of streamflow observed at a given time and location that can be attributed to groundwater discharge to the stream. This lead to various baseflow separation approaches, such as the traditional, event-based graphical (Barnes, 1939; Hewlett and Hibbert, 1963, 1967; Szilagyi and Parlange, 1998) methods, which have recently been replaced by automated, filter-based algorithms (Nathan and McMahon, 1990; Chapman, 1991, 1999; Arnold et al., 1995; Arnold and Allen, 1999) that provide continuous baseflow separation in time. The significant advantage of these approaches is that they only require stream discharge data. Their weaknesses are that either they are tedious to construct and not continuous (characteristic of the former), or continuous but then lack any physical basis whatsoever (typical of the latter), combined with a significant degree of arbitrariness in the choice of the filter parameter value. Recently, there were some attempts reported, aimed at reducing the degree of uncertainty in choosing the proper filter parameter value (Szilagyi et al., 2003; Szilagyi, 2004b). A third approach to baseflow separation relies on some sort of a conceptual model of the rainfall–runoff relationship (e.g. Jakeman et al., 1990; Jakeman and Hornberger, 1993; Furey and Gupta, 2001, 2003; Young, 2001), sometimes combined with analytical solutions of the simplified Boussinesq equation (Pauwels et al., 2002; Paniconi et al., 2003; Troch et al., 2003, 2004; Hilberts et al., 2004). While these latter approaches are exciting, they all require information on precipitation, which is often times inadequate or not available at all.

One way the above techniques can be verified or assisted in their parameter optimization (Robson et al., 1992) is by comparison to flow separation results using isotope or chemical tracers, because these latter are, in principle, capable of differentiating between stream- and groundwater, in terms of ‘event’ and ‘pre-event’ water in the catchment relative to a storm (Sklash and Folvolden, 1979; Rice and Hornberger, 1998).

Below a physically based approach is described for an assessment of stream–aquifer interactions between a given reach of the stream and its adjacent aquifer. It may become a complementary or in certain cases an alternative method to tracer techniques. The proposed method, similar to the chemical or isotope mixing techniques, is based on mass conservation, but unlike them, it requires only the most basic, routinely available measurement, i.e. stream discharge.

## Derivation of the Discrete Linear Cascade Model

One-dimensional open channel flow is described by the St-Venant equations (Henderson, 1966) made up of the continuity and momentum equations. The former for a stream reach with no lateral inflow can be written as

$$\frac{\partial A}{\partial t} + \frac{\partial Q}{\partial x} = 0 \quad (1)$$

where  $A(x,t)$  is the wetted cross-sectional area,  $Q(x,t)$  is the mean cross-sectional streamflow rate (discharge),  $x$  and  $t$  are spatial and temporal coordinates. The momentum equation is

$$S_f = S_0 - \frac{\partial h}{\partial x} - \frac{Q}{gA} \frac{\partial(Q/A)}{\partial x} - \frac{1}{g} \frac{\partial(Q/A)}{\partial t} \quad (2)$$

where  $S_f(x,t)$  and  $S_0(x)$  are the friction and channel-bed slopes, respectively,  $h(x,t)$  is the mean cross-sectional water depth, and  $g$  is the gravitational acceleration. The friction slope is often written as

$$S_f = Q^2 A^{-2} n_0^2 R^{-4/3} \quad (3)$$

where  $R(x,t)$  is the hydraulic radius ( $=AP^{-1}$ ,  $P(x,t)$  being the wetted perimeter of the channel), and  $n_0(x)$  the Manning coefficient.

Neglecting the acceleration terms, i.e. the last two terms on the right-hand-side, of Eq. (2) and combining it with Eq. (1) yields the nonlinear diffusion wave equation (Henderson, 1966)

$$\frac{\partial Q}{\partial t} + c(Q) \frac{\partial Q}{\partial x} = D(Q) \frac{\partial^2 Q}{\partial x^2} \quad (4)$$

where  $c$  is the wave celerity, and  $D$  is a diffusion coefficient.

The linear kinematic wave equation of flow routing derives by further neglecting the diffusion term in Eq. (4), and assuming that the wave celerity is constant ( $=c_k$ )

$$\frac{\partial Q}{\partial t} + c_k \frac{\partial Q}{\partial x} = 0 \quad (5)$$

Using a backward-difference scheme in the spatial derivative, Eq. (5) can be written as (Szollosi-Nagy, 1982, 1989)

$$\begin{aligned} \frac{\partial Q(x_j, t)}{\partial t} &= -c_k \frac{Q(x_j, t) - Q(x_{j-1}, t)}{\Delta x} \\ &= \frac{c_k}{\Delta x} Q(x_{j-1}, t) - \frac{c_k}{\Delta x} Q(x_j, t) \end{aligned} \quad (6)$$

with  $x_j = j\Delta x$ ; where  $\Delta x$  is the constant length scale of the spatial discretization, and  $j = 1, 2, \dots, n$ . Here  $n$  is the number of so-derived stream subsections of a stream reach. One may define a vector variable as  $\mathbf{Q}(t) = [Q(x_1, t), Q(x_2, t), \dots, Q(x_n, t)]' = [Q_1(t), Q_2(t), \dots, Q_n(t)]'$  where the prime denotes the transpose. By denoting the inflow to the reach as  $\mathbf{u}(t) = Q_0(t)$ , Eq. (6) with  $j = 1, \dots, n$  transforms into

$$\begin{bmatrix} \frac{dQ_1(t)}{dt} \\ \frac{dQ_2(t)}{dt} \\ \vdots \\ \frac{dQ_n(t)}{dt} \end{bmatrix} = \begin{bmatrix} -\frac{c_k}{\Delta x} & 0 & \cdots & 0 \\ \frac{c_k}{\Delta x} & -\frac{c_k}{\Delta x} & \ddots & \vdots \\ & \ddots & \ddots & 0 \\ 0 & & \frac{c_k}{\Delta x} & -\frac{c_k}{\Delta x} \end{bmatrix} \begin{bmatrix} Q_1(t) \\ Q_2(t) \\ \vdots \\ Q_n(t) \end{bmatrix} + \begin{bmatrix} \frac{c_k}{\Delta x} \\ 0 \\ \vdots \\ 0 \end{bmatrix} \mathbf{u}(t) \quad (7)$$

The outflow,  $\mathbf{y}(t) = Q_n(t)$  of the reach can be obtained as

$$\mathbf{y}(t) = [0, 0, \dots, 1] \mathbf{Q}(t) \quad (8)$$

When a subreach is considered as a linear storage element, then its outflow,  $Q_i(t)$ , is directly proportional to the stored water volume,  $S_i(t)$ , within the element, i.e.  $Q_i(t) = kS_i(t)$ , where  $k = \frac{c_k}{\Delta x}$  is the proportionality constant or storage coefficient (i.e. the inverse of the mean storage time). Eqs. (7) and (8) with the  $Q_i(t) = kS_i(t)$  substitution transform into

$$\begin{bmatrix} \frac{dS_1(t)}{dt} \\ \frac{dS_2(t)}{dt} \\ \vdots \\ \frac{dS_n(t)}{dt} \end{bmatrix} = \begin{bmatrix} -k & 0 & \dots & 0 \\ k & -k & \ddots & \vdots \\ & \ddots & \ddots & 0 \\ 0 & & k & -k \end{bmatrix} \begin{bmatrix} S_1(t) \\ S_2(t) \\ \vdots \\ S_n(t) \end{bmatrix} + \begin{bmatrix} 1 \\ 0 \\ \vdots \\ 0 \end{bmatrix} u(t) \quad (9)$$

and

$$y(t) = \mathbf{H}\mathbf{S}(t) \quad (10)$$

respectively, where  $\mathbf{H} = [0, 0, \dots, k]$ . Eqs. (9) and (10) constitute the state-space representation of the continuous Kalinin–Milyukov–Nash (KMN)-cascade (Szilagyi, 2003b). Eq. (9) can be more succinctly written as

$$\dot{\mathbf{S}}(t) = \mathbf{F}\mathbf{S}(t) + \mathbf{G}u(t) \quad (11)$$

where the dot denotes the temporal change in the state variable,  $\mathbf{S}(t)$ ;  $\mathbf{F}$  and  $\mathbf{G}$  are the system matrix and input-distribution vector, respectively. Eqs. (10) and (11) represent the output and state equations of a linear, continuous, dynamic system with time-invariant coefficient matrices/vectors (Szollosi-Nagy, 1982).

Let us now consider the nature of streamflow data. No matter how stream discharge is derived, it eventually becomes a discrete value on the digital computer. As a consequence, it is desirable to transform the continuous KMN-cascade into its discrete form, making it compatible with its discrete input. Szollosi-Nagy (1982) performed the discretization in a pulse-data system, where it is assumed that the discretely sampled variable keeps its last value until a new sampling is available. This data system originates from electrical engineering and it is not the best choice with continuously changing variables, such as flow rate. Szilagyi (2003b) performed the discretization of Eq. (11) in a sample-data system framework, where it is assumed that the change in the variable's value can be essentially considered as linear between subsequent samples. Below we show this latter result for a constant  $\Delta t$  sampling interval. The solution of Eq. (11) in the sample-data system becomes (Szilagyi, 2003b)

$$\mathbf{S}_{t+\Delta t} = \Phi \mathbf{S}_t + \Gamma^{(1)} u_{t+\Delta t} + \Gamma^{(2)} u_t \quad (12)$$

where  $\Phi$  is the state-transition matrix,  $\Gamma^{(1)}$  and  $\Gamma^{(2)}$  are the input-transition vectors. The time reference as an index is meant to show the temporally discrete nature of the model. The  $n \times n$  state-transition matrix is defined as

$$\Phi = \begin{bmatrix} e^{-k\Delta t} & 0 & \dots & 0 \\ k\Delta t e^{-k\Delta t} & e^{-k\Delta t} & \ddots & \vdots \\ \vdots & \vdots & \ddots & 0 \\ \frac{(k\Delta t)^{n-1}}{(n-1)!} e^{-k\Delta t} & \frac{(k\Delta t)^{n-2}}{(n-2)!} e^{-k\Delta t} & \dots & e^{-k\Delta t} \end{bmatrix} \quad (13)$$

while the input-transition vectors are

$$\Gamma^{(1)} = \begin{bmatrix} \frac{1}{k} \frac{\Gamma(1, k\Delta t)}{\Gamma(1)} \left[ 1 + \frac{e^{-k\Delta t}}{\Gamma(1, k\Delta t)} - \frac{1}{k\Delta t} \right] \\ \frac{1}{k} \frac{\Gamma(2, k\Delta t)}{\Gamma(2)} \left[ 1 + \frac{k\Delta t e^{-k\Delta t}}{\Gamma(2, k\Delta t)} - \frac{2}{k\Delta t} \right] \\ \vdots \\ \frac{1}{k} \frac{\Gamma(n, k\Delta t)}{\Gamma(n)} \left[ 1 + \frac{(k\Delta t)^{n-1} e^{-k\Delta t}}{\Gamma(n, k\Delta t)} - \frac{n}{k\Delta t} \right] \end{bmatrix} \quad (14)$$

and

$$\Gamma^{(2)} = \begin{bmatrix} \frac{1}{k} \frac{\Gamma(1, k\Delta t)}{\Gamma(1)} \left[ \frac{1}{k\Delta t} - \frac{e^{-k\Delta t}}{\Gamma(1, k\Delta t)} \right] \\ \frac{1}{k} \frac{\Gamma(2, k\Delta t)}{\Gamma(2)} \left[ \frac{2}{k\Delta t} - \frac{k\Delta t e^{-k\Delta t}}{\Gamma(2, k\Delta t)} \right] \\ \vdots \\ \frac{1}{k} \frac{\Gamma(n, k\Delta t)}{\Gamma(n)} \left[ \frac{n}{k\Delta t} - \frac{(k\Delta t)^{n-1} e^{-k\Delta t}}{\Gamma(n, k\Delta t)} \right] \end{bmatrix} \quad (15)$$

The function, denoted by  $\Gamma$  within  $\Gamma^{(1)}$  and  $\Gamma^{(2)}$ , is the incomplete (with two arguments, i.e.  $\Gamma(a, \xi) = \int_0^\xi e^{-t} t^{a-1} dt$ ), or complete (with one argument, i.e.  $\Gamma(a) = \int_0^\infty e^{-t} t^{a-1} dt$ ) gamma-function, respectively. Note that all system matrices/vectors (i.e.  $\Phi$ ,  $\Gamma^{(1)}$  and  $\Gamma^{(2)}$ ) are time-invariant and only depend on the magnitude of the sampling interval,  $\Delta t$ ; and that the output equation Eq. (10) becomes unchanged, as it is algebraic. Eqs. (10) and (12) constitute the Discrete Linear Cascade Model (DLCM) in a sample-data system framework, and are to be used for assessing stream–aquifer interactions after some further modifications.

To demonstrate the applicability of DLCM, the St-Venant equations were numerically integrated over a hypothetical stream reach of 2000 km in length, having a uniform, rectangular channel cross-section of 300 m in width, a constant Manning coefficient of 0.035, and an also constant channel bottom slope of 0.0002. The initial permanent water depth,  $h_0$ , was set to 5 m. The upper boundary condition was given by

$$h(x=0, t) = h_0 + \frac{1 - \cos\left(\frac{2\pi}{t_m} t\right)}{1 - \cos\left(\frac{2\pi t_c}{t_m}\right)} \times \exp\left\{\frac{2\pi}{t_m} \cot\left[\frac{\pi t_c}{t_m}(t_c - t)\right]\right\} \quad 0 \leq t \leq t_m$$

$$h(x=0, t) = h_0 \quad t > t_m \quad (16)$$

with  $t_m = 2 d = 172, 800$  s; and  $t_c = 0.5 d = 43, 200$  s. The lower boundary condition at  $L = 2000$  km was given by a permanent rating curve. To make sure that the somewhat artificial boundary conditions have minimal effect on the simulation, the stream reach where the numerical results were compared to the flow routing results of DLCM was chosen between  $L = 900$  and 1000 km, thus having a 100 km reach for flow routing comparisons. Input water depth values to the chosen reach were provided by the numerical solution of the St-Venant equations, which also served as “ground truth” water depth values at the outlet of the reach as well, against which the flow routing results were compared.

The reason for specifying water depth values over discharge values in the demonstration is that the primary information on streamflow is in the form of stage measurements, which are subsequently transformed into discharge values. This transformation can be obtained by the Jones formula (1916)

$$Q = Q_0 \sqrt{1 + \frac{1}{S_0 C_k} \frac{\partial h}{\partial t}} \quad (17)$$

where  $Q_0$  is the permanent flow rate belonging to stage  $h$ . Note that in Eq. (17) only the temporal change of  $h$  is present; thus it does not matter whether  $h$  denotes the actual

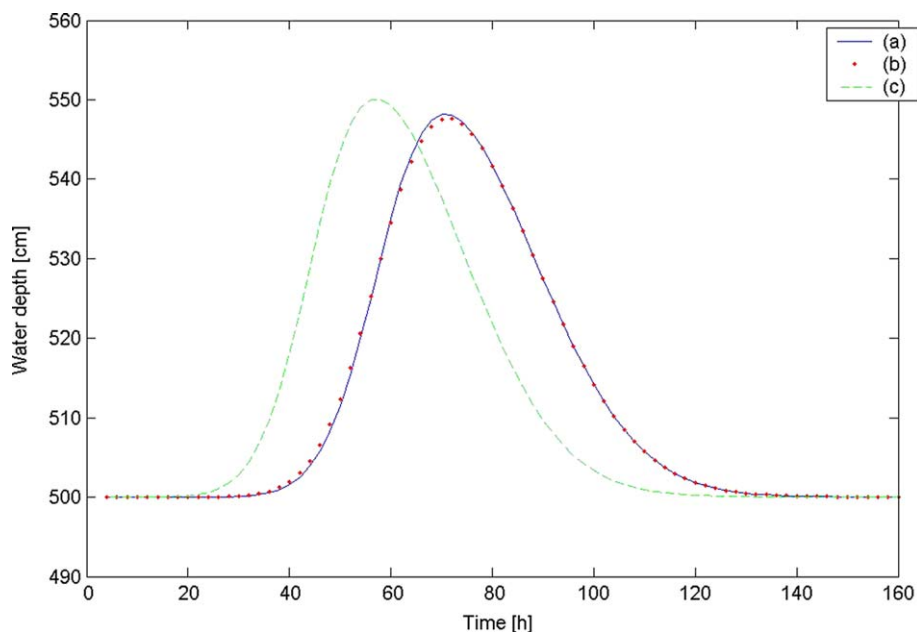


**Figure 1** Numerical solution of the St-Venant equations and flow routing results using DLCM for a 100-km long rectangular channel reach. (a) Downstream mean water depth given by the St-Venant equations; (b) DLCM-estimated downstream mean water depth ( $n = 7$ ,  $k = 0.51 \text{ h}^{-1}$ ); (c) upstream mean water depth.

water depth, or rather stage, which, of course, is water depth over an arbitrary datum. The  $Q_0$  versus  $h$  relationship is provided by Eq. (3), where during permanent conditions  $S_f = S_0$ . Note that during flow routing with the DLCM, Eq. (17) is explicit for the reach inflow rate, but becomes implicit for  $h$  at the stream outlet.

Optimization of the DLCM parameters of  $n$  and  $k$  was achieved by systematic trial and error analysis, and  $c_k$  in Eq. (17) was estimated (since in practice the celerity is not known) by the chosen parameter values as

$$c_k = \frac{L_r}{nk^{-1}} = \frac{kL_r}{n} \quad (18)$$

where  $L_r = 100 \text{ km}$  is the length of the reach.

Fig. 1 displays the up- and downstream water-depth hydrograph as given by the numerical integration of the St-Venant equations and the optimized flow routing results with  $n_{\text{opt}} = 7$ ,  $k_{\text{opt}} = 0.51 \text{ h}^{-1}$ . As is expected, the linear model smears out the flood-wave a bit more than what actually occurs due to the neglected acceleration terms in Eq. (2). Note also that indeed the DLCM is capable of reproducing dispersion of the flood-wave to a rather high degree, even though it is derived from the kinematic wave equation. This feature of DLCM stems from numerical dispersion which is brought about when the spatial derivatives in Eq. (5) are approximated with a finite difference scheme. This way the DLCM, i.e. Eq. (12) combined with Eq. (10), can be considered an approximate solution of the linear diffusion wave equation.

### Inversion of the Discrete Linear Cascade Model

The inversion of DLCM, i.e. determining the inflow to the reach having information of the outflow, generally consists of two steps. First the initial state,  $S_0$ , is calculated, which

means estimating the stored water volumes in each linear storage element, and then, with the help of this information, the inflow series. The first step, for an  $n$ -cascade requires  $n$  pairs of inflow–outflow data in the pulse-data system, and  $n + 1$  inflow, and  $n$  outflow values in the sample-data system, employed here. Identification of the initial state can be side-stepped when inflow to the reach is not known at all. It is so because a typical stream reach with relatively small mean storage time (which means a large  $k$  value), ‘forgets’ its initial state very fast. In fact, the Danube (Europe’s second largest river after the Volga in Russia), for which stream–aquifer interactions will be demonstrated below, has a memory of about a couple of weeks at most, meaning that after this period the outflow from a reach even 100 km in length does not depend on the initial state. At the same time a good initial guess at  $S_0$ , even if it is not entirely correct, as in the case in the presence of stream–aquifer interactions, shortens this ‘spin-up’ period significantly. That is why the required calculations are displayed below.

For a reach with no lateral in- or outflow, the initial state estimation in a pulse-data system was derived by Szollosi-Nagy (1987). Here we show the equations for a sample-data system (Szilagyi, 2003b)

$$S_0 = \theta^{-1} \mathbf{m} \quad (19)$$

where  $\theta$  is an  $n \times n$ , so-called, observability matrix (Meditch, 1969)

$$\theta = \begin{bmatrix} \mathbf{H}\Phi \\ \mathbf{H}\Phi^2 \\ \vdots \\ \mathbf{H}\Phi^n \end{bmatrix} \quad (20)$$

and  $\mathbf{m}$  is the measurement vector

$$\mathbf{m} = \begin{bmatrix} y_{1\Delta t} - (h_1^{(2)}u_{0\Delta t} + h_1^{(1)}u_{1\Delta t}) \\ y_{2\Delta t} - (h_2^{(2)}u_{0\Delta t} + h_2^{(1)}u_{1\Delta t} + h_1^{(2)}u_{1\Delta t} + h_1^{(1)}u_{2\Delta t}) \\ \vdots \\ y_{n\Delta t} - \sum_{j=0}^{n-1} (h_{n-j}^{(2)}u_{j\Delta t} + h_{n-j}^{(1)}u_{(j+1)\Delta t}) \end{bmatrix} \quad (21)$$

Note that indices containing  $\Delta t$  are temporal ones. Here  $h_j^{(i)} = \mathbf{H}\Phi^{j-1}\Gamma^{(i)}$ , where  $i$  assumes a value either unity or two.

Having an estimate of  $\mathbf{S}_0$ , inversion of the combined equations of (10) and (12)

$$y_{\Delta t} = \mathbf{H}\Phi\mathbf{S}_0 + \mathbf{H}\Gamma^{(1)}u_{\Delta t} + \mathbf{H}\Gamma^{(2)}u_0 \quad (22)$$

yields for the inflow at  $t = \Delta t$

$$u_{\Delta t} = \frac{1}{h_1^{(1)}}(y_{\Delta t} - \mathbf{H}\Phi\mathbf{S}_0 - h_1^{(2)}u_0) \quad (23)$$

which shows that in the sample-data system (unlike in the pulse-data system), not only  $\mathbf{S}_0$  must be known, but  $u_0$  as well. Note that the estimation of  $\mathbf{S}_0$  assumes that  $u_0$  is known. When it is not so, knowing  $u_0$  or not makes no difference, since the estimated inflow values during the spin-up period should be discarded anyway.

Together with the  $u_{\Delta t}$  estimation,  $\mathbf{S}_{\Delta t}$  must be calculated as well

$$\mathbf{S}_{\Delta t} = \Phi\mathbf{S}_0 + \Gamma^{(1)}u_{\Delta t} + \Gamma^{(2)}u_0 \quad (24)$$

Once  $\mathbf{S}_{\Delta t}$  is obtained,  $u_{2\Delta t}$  is provided by

$$u_{2\Delta t} := \frac{1}{h_1^{(1)}}(y_{2\Delta t} - \mathbf{H}\Phi\mathbf{S}_{\Delta t} - h_1^{(2)}u_{\Delta t}) \quad (25)$$

and so on.

Before the inversion can be applied to assess stream–aquifer interactions the following considerations have to be made. Possible lateral in- and outflow of the stream reach must somehow be incorporated into DLCM which so far permits inflow to only the first linear storage element in the cascade, and outflow from the last one (single input–single output [SISO]). The modified model that allows for stream–aquifer interactions can be written the following way

$$\mathbf{S}_{t+\Delta t} = \Phi\mathbf{S}_t + \Gamma^{(1)}u_{t+\Delta t} + \Gamma^{(2)}u_t + \omega q_t \quad (26)$$

where the new, additional  $n \times 1$  input-transition vector's  $i$ th component becomes

$$\omega_i = \sum_{j=1}^i \gamma_j \quad (27)$$

with  $\gamma_j$  being the  $j$ th component of the input-transition vector of the original SISO model when written in a pulse-data system framework. Note that in the pulse-data system at time  $t$ ,  $u_{t+\Delta t}$  is assumed to be equal to  $u_t$ , thus the two input-transition vectors,  $\Gamma^{(1)}$  and  $\Gamma^{(2)}$ , collapse into a single vector,  $\Gamma$ , whose  $j$ th component is

$$\gamma_j := \frac{1}{k} \frac{\Gamma(j, k\Delta t)}{\Gamma(j)} \quad (28)$$

which is the often-called scaled incomplete gamma function, times  $k^{-1}$ . The present formulation of Eq. (26) assumes that possible groundwater contribution to the stream is con-

stant during the sampling interval,  $\Delta t$ . This is an assumption of convenience which not only makes the final model simpler, but also allows for an explicit expression of  $q_t$

$$q_t = \frac{1}{\mathbf{H}\omega} (y_{t+\Delta t} - \mathbf{H}\Phi\mathbf{S}_t - h_1^{(1)}u_{t+\Delta t} - h_1^{(2)}u_t) \quad (29)$$

which is the sought-after flux-exchange between stream and aquifer. Note that the model assumes not only a constant  $q_t$  during the sampling interval, but also the same value along the entire reach of the stream; in other words, the same  $q_t$  rate simultaneously to each linear storage element. This restriction is necessary for Eq. (29) to be fully determined and it may become a potential problem only for extremely long stream-reaches having a larger length than the typical spatial scale of a flood-wave, since then different parts of the reach may experience largely different stream water levels and consequently greatly differing lateral flux exchange rates.

To complete the inversion, Eq. (26) must be evaluated with  $q_t$  of Eq. (29) and the resulting  $\mathbf{S}_{t+\Delta t}$  value used in

$$q_{t+\Delta t} = \frac{1}{\mathbf{H}\omega} (y_{t+2\Delta t} - \mathbf{H}\Phi\mathbf{S}_{t+\Delta t} - h_1^{(1)}u_{t+2\Delta t} - h_1^{(2)}u_{t+\Delta t}) \quad (30)$$

to obtain the groundwater flux rate at the next time-step.

## Demonstration of inverse modeling and discussion of results

Assessment of stream–aquifer interactions is demonstrated on a 85.9 km stretch of the Danube River in Hungary. Information of inflow to the reach at Budapest, as well as outflow from it at Dunafoldvar (Fig. 2), is obtained in the form of stage readings twice daily (6 a.m. and 6 p.m.) for the period of 1995–1997. Stage measurements were transformed into flow rates through the application of permanent rating curves (Fig. 3), together with Eqs. (17) and (18), using optimized DLCM parameters of  $n = 2$ ,  $k = 2.2 \text{ d}^{-1}$ .

Optimization was achieved by employing a weighted root mean square error objective function for the measured and modeled stages, where the weights were given by the magnitude of the observed stage. This way the model was forced to give less importance to low-flow stages where the influence of lateral inflow is expected to be larger (Fig. 4) in both relative and absolute terms, and give more weights to flood-waves where this interaction is expected to be less significant, however not negligible due to possible bank storage effects, as will be shown below. Note that the model in its parameter optimization mode does not account for lateral inflow whose rate is unknown yet. The basic tenet here is that the model, in the absence of lateral flux exchange, *must* provide rather accurate simulation of the outflow. When this is violated, the present assumption claims, it must be due chiefly to lateral flux exchanges and only negligibly to inaccuracies in the rating curves and/or the flow routing technique itself (Fig. 1).

Another important point to raise is that even if somehow the lateral flux exchange rate would be known in advance and included in the flow routing, it would not change the result of the parameter optimization, as was demonstrated by Szilagyı (2004a) for a section of the Danube that included the present study reach. This is so due to Eq. (18), i.e.



Figure 2 The Danube River in Hungary with the up- and downstream gaging station locations shown.

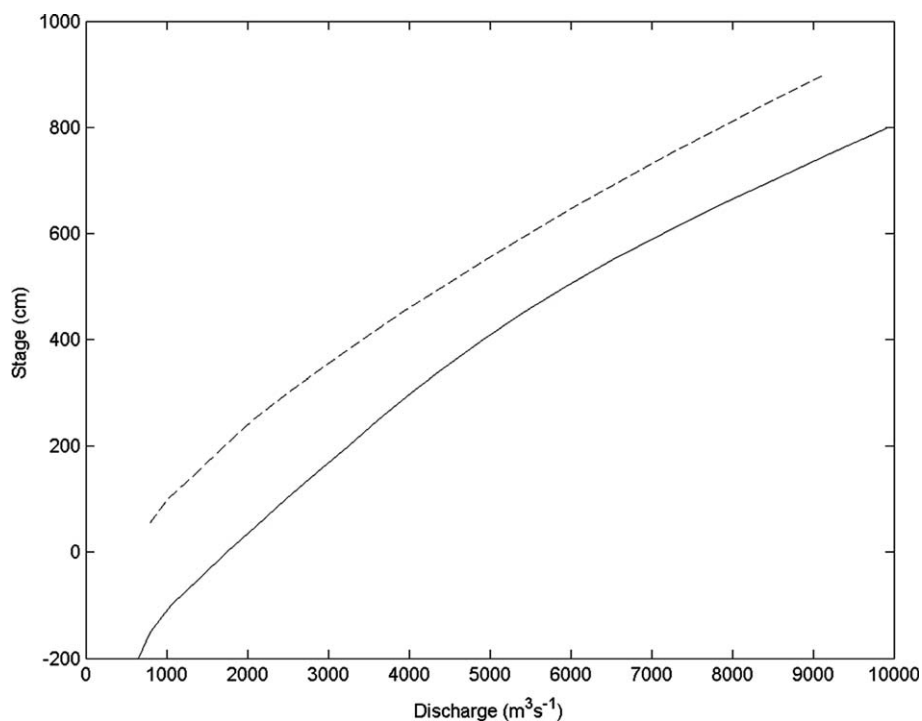


Figure 3 Permanent rating curves employed at Budapest (intermittent) and Dunafoldvar.

the two parameters of DLCM determine the flood-wave celerity, which remains practically the same with or without stream–groundwater interactions under not too extreme conditions, i.e. when stream gains or losses do not dominate streamflow. It is also true that the two parameters may change their values in a way that the celerity stays unchanged. In fact, the smaller the value of  $n$  for a given celerity, the higher the degree of dispersion of the flood-wave, and in that, bank storage can play a role, but generally to a rather limited level (Szilagyi, 2004a).

The chosen stream reach of the Danube has no tributaries, so lateral in- and outflow of the reach practically occurs in the form of stream–aquifer interactions. There is some minor flow diversion at about the halfway point of the reach

to irrigation canals, but virtually no irrigation takes place using water from these canals. Irrigated land area all over Hungary is minuscule, mostly because there are only very few years per decade when additional water to precipitation would be needed for typical, traditional agricultural crops in the region. Mean annual precipitation is about 700 mm in central Hungary with a relatively even distribution throughout the year.

From Fig. 4 the presence of groundwater discharge to the stream is evident, especially at low stages, where the DLCM-simulated stages are always below the observed ones. The mean flow rate over the study period is  $2504 \text{ m}^3 \text{ s}^{-1}$  at Budapest, and  $2641 \text{ m}^3 \text{ s}^{-1}$  at Dunafoldvar, so the study reach clearly gains water from the adjacent aquifer.

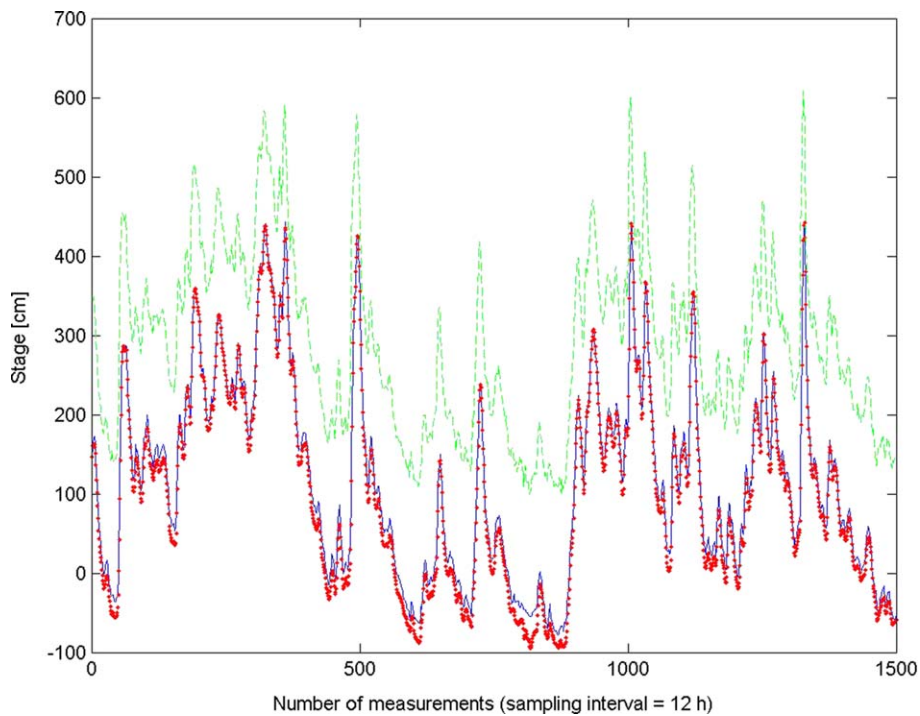


**Figure 4** Twice daily stages of the Danube at Budapest (intermittent line) and Dunafoldvar. The crosses designate the DLCM-estimated ( $n = 2$ ,  $k = 2.2 \text{ d}^{-1}$ ) stage values at Dunafoldvar. Time period: January 1, 1995 to January 19, 1997.

Fig. 5 displays the result of model inversion as described by Eqs. (26)–(30). Rather than showing the original, high variance time-series of the inversion, Fig. 5 contains a filtered flux time-series, using a running average of 5 days in both the forward and backward directions (in order to pre-

serve phase), as described by the ‘filtfilt’ function of MATLAB. This is justified because natural processes, such as streamflow, often show characteristics of highly damped systems which means that the output, in our case outflow, is significantly smoother than the input/inflow. Flow routing

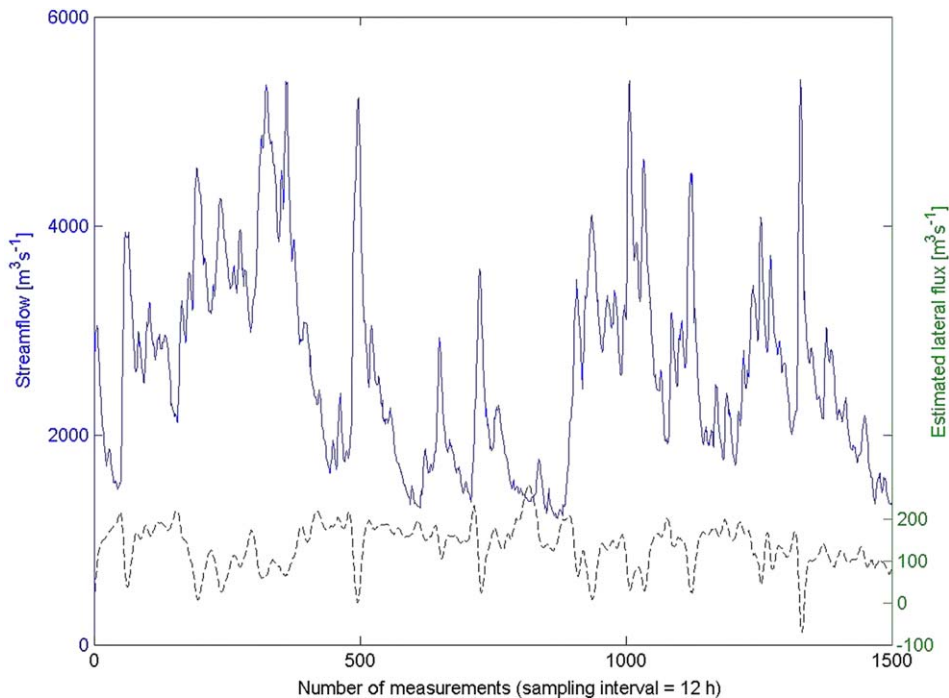


**Figure 5** Jones-formula-derived flowrate at Dunafoldvar (solid line) and estimated flux exchange rate between stream and aquifer. Time period: January 1, 1995 to January 19, 1997.

this way can be considered as a smoothing process, while the inverse of it as an amplification. From this it follows that a small irregularity due to measurement or model errors in the output will cause a relatively large error in the estimated input value during the inversion. Also, rather than showing a staircase function (since Eq. (26) assumes that  $q_t$  stays constant during the sampling interval) for the estimated lateral flux rates, the discrete values were connected with straight lines out of convenience.

The estimated lateral flux rates display a clear inverse relationship (a linear correlation coefficient of  $-0.68$ ) with streamflow: the higher the streamflow rate, the lower the discharge of groundwater to the stream, and vice versa. Note that when the increase in the streamflow rate is very sudden, the Danube will temporarily release more water to the adjacent aquifer through its banks than what it gains from the groundwater, producing negative flux values. The rate of flooding in the stream is indeed the dominant factor rather than its magnitude, since in Fig. 5 there are two other flood-waves (at about 500 and 1000) with almost the same magnitude and neither of them produced significant reversed fluxes. This is so because the study reach is supplied by a continuous unconfined, sand aquifer from the east (the authors have no information of the aquifer west of the Danube) with a groundwater divide 35–50 m above the mean stage of the Danube at a distance of about 50 km from the river (Szilagyi and Vorosmarty, 1997). Consequently, the Danube, even at its highest stage, should constantly gain water were short-lived, dynamic changes in stream stage neglected.

The importance of such dynamics is highlighted by the help of a numerical model reconfirming the findings of the proposed inversion. Stream–aquifer interactions were simulated by a finite element model that numerically integrated the combined unsaturated/saturated flow equation (Lam et al., 1987; Szilagyi, 2003a)

$$\frac{\partial}{\partial y} \left[ k(\Psi) \frac{\partial H}{\partial y} \right] + \frac{\partial}{\partial z} \left[ k(\Psi) \frac{\partial H}{\partial z} \right] = m\chi \frac{\partial H}{\partial t} \quad (31)$$

where  $k$  (a function of  $\Psi$ , the suction/pressure head) denotes both unsaturated and saturated hydraulic conductivities;  $m$  is the slope of the water retention curve, which becomes the coefficient of volume change in the saturated zone;  $\chi$  is the unit weight of water;  $H$  is the total hydraulic head;  $y$  is spatial coordinate in a direction perpendicular to the stream, while  $z$  is the same in the vertical direction. Fig. 6 displays the schematic of an aquifer interacting with

a stream of prescribed changing stages, starting with a steady initial state of drawdown. In the numerical model the aquifer is assigned a physical texture of sand (see Szilagyi, 2003a for the ensuing material properties), and has a width ( $B$ ) of 20 m. The groundwater is kept at a constant elevation of 4 m at the groundwater divide ( $B = 20$  m) in order to emulate the effect of aquifer recharge; and during the steady, initial conditions stream water was kept at 0.5 m above the channel bottom; this latter is situated 1 m above a horizontal impervious layer. Stream half-width is 1 m and the ground surface is at 5 m.

In the first scenario a slow, while in the second one, a fast, flood event was simulated. Stream stages could not be changed continuously in time in the model, because that would have implied changing the boundary conditions continuously in time as well. Rather, stages were kept constant for a given time period ( $\Delta t = 0.1$  d) and then changed instantaneously from one value to the next. Flux exchanges across the stream bottom and across the stream bank could be monitored separately. Fig. 7 displays the resulting simulated interactions between stream and adjacent aquifer. Similar to the inversion results, bank storage of stream water is related to the speed of stage increase in the stream.

Continuous baseflow separation is made possible by routing the water gained by the stream along the study reach. This is possible because the model is linear; consequently inflow to the reach can be routed in any arbitrary increments provided mass is conserved. Fig. 8 displays the results of this flow routing. When the stream loses water (at about 1350 in Fig. 5), the negative  $q_t$  value was replaced by zero during the routing. Strictly speaking, the negative  $q_t$  value ought to be multiplied by a fraction equal to the proportion of baseflow supplied by the reach to total streamflow (since the stream loses baseflow too), but the difference in the outcome would be imperceptible. Note that only baseflow that was gained along the stream reach, defined by the up- and downstream gaging stations, can be separated from streamflow. Certainly, if groundwater contribution to the flow upstream of the inflow gaging station is negligible, as may be the case for certain headwater or partially urbanized catchments, the routing provides full separation of groundwater from stream water in the classical baseflow separation sense. River reaches downstream of reservoirs are especially suited for studying stream–aquifer interactions with the present technique because the typically long residence time of water in the reservoir detaches any such

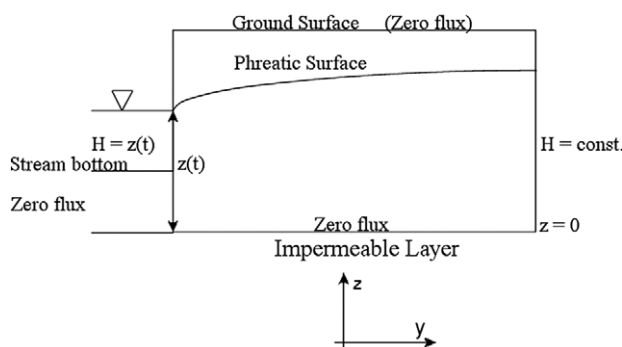
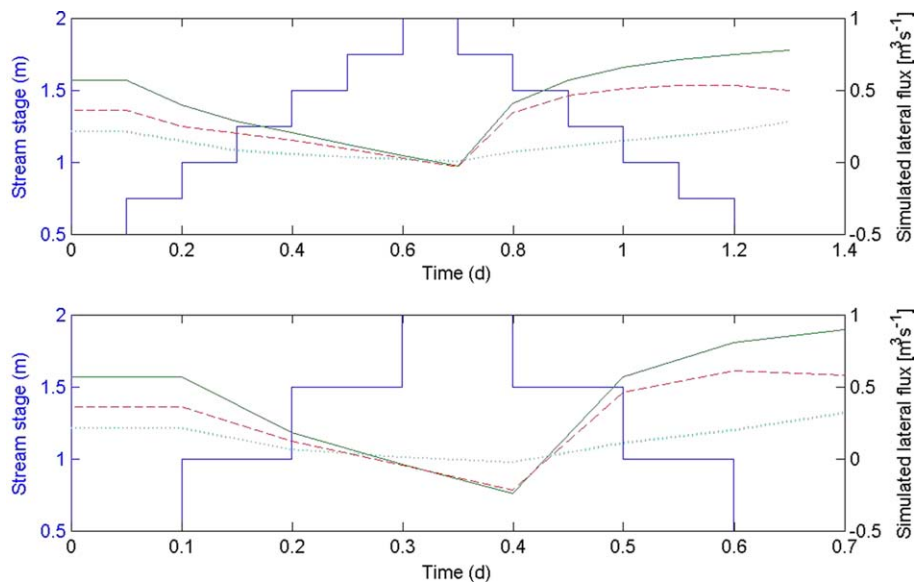
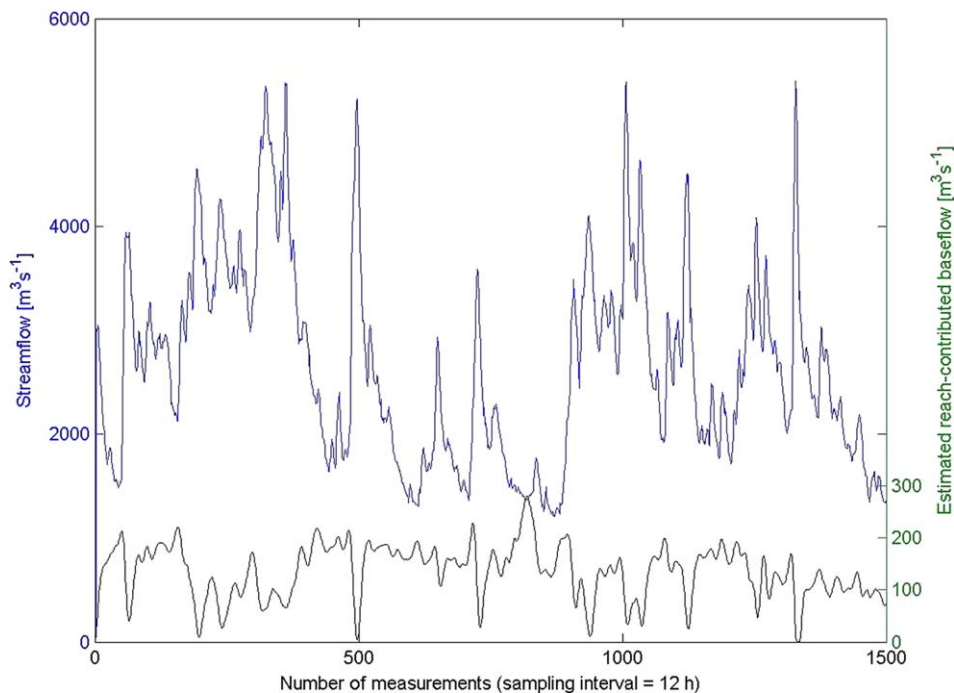


Figure 6 Schematic of the stream–aquifer system with the initial and boundary conditions shown.



**Figure 7** Prescribed stream stages (stairs), numerical simulation results of lateral fluxes across the stream bottom (dots) and stream bank (intermittent) and their sum. Top panel: slow flood-wave case; bottom panel: quick flood-wave case. Flux is positive when the stream is gaining water from the aquifer.



**Figure 8** Streamflow and estimated reach-contributed baseflow time-series at Dunafoldvar, January 1, 1995 to January 19, 1997. Baseflow input to the reach is from Fig. 5 which was subsequently routed along the study reach.

dynamic effects from the reservoir outflow serving as input to the above analysis. This way, full baseflow separation at a given gaging station of a stream can be achieved by sequentially routing groundwater gain between two adjacent gaging stations starting at an appropriate (provided such exists) upstream gaging station of the stream. Again, because the model is linear, tributary inflow can easily be dealt with by routing its flow to the target gaging station simultaneously with the main channel routing and summing

the results of the two flow routings. For example, if two streams join, having each a gaging station, then the flow at the gaging station below their confluence is to be obtained by two separate cascades, meaning the simultaneous optimization of two  $n$  and two  $k$  values. The simple state-space structure of DLCM with its linearity makes such calculations easy and extremely fast. That is why DLCM is used operatively in Hungary for real-time flow forecasting over a network of 400-plus gaging stations.

## Acknowledgement

The editorial comments of Charles Flowerday of the University of Nebraska are greatly appreciated.

## References

- Arnold, J.G., Allen, P.M., 1999. Automated methods for estimating baseflow and ground water recharge from streamflow records. *J. Am. Water Resour. Assoc.* 35 (2), 411–424.
- Arnold, J.G., Allen, P.M., Muttiah, R., Bernhardt, G., 1995. Automated baseflow separation and recession analysis techniques. *Ground Water* 33 (6), 1010–1018.
- Barnes, B.S., 1939. The structure of discharge recession curves. *Transact. AGU* 20, 721–725.
- Brutsaert, W., Lopez, J.P., 1998. Basin-scale geohydrologic drought flow features of riparian aquifers in the southern Great Plains. *Water Resour. Res.* 34 (2), 233–240.
- Brutsaert, W., Nieber, L.L., 1977. Regionalized drought flow hydrographs from a mature glaciated plateau. *Water Resour. Res.* 13, 637–643.
- Chapman, T.G., 1991. Comment on evaluation of automated techniques for baseflow and recession analysis by R.J. Nathan and T.A. McMahon. *Water Resour. Res.* 27 (7), 1783–1784.
- Chapman, T.G., 1999. A comparison of algorithms for stream flow recession and baseflow separation. *Hydrol. Process.* 13, 701–714.
- Furey, P.R., Gupta, V.K., 2001. A physically based filter for separating base flow from streamflow time series. *Water Resour. Res.* 37 (11), 2709–2722.
- Furey, P.R., Gupta, V.K., 2003. Tests of two physically based filters for base flow separation. *Water Resour. Res.* 39 (10), art. # 1297.
- Henderson, F.M., 1966. *Open Channel Flow*. MacMillan, New York.
- Hewlett, J.D., Hibbert, A.R., 1963. Moisture and energy considerations within a sloping soil mass during drainage. *J. Geophys. Res.* 64, 1081–1087.
- Hewlett, J.D., Hibbert, A.R., 1967. Factors affecting the response of small watersheds to precipitation in humid areas. In: Sopper, W.E., Lull, H.W. (Eds.), *International Symposium on Forest Hydrology*. Pergamon Press, Oxford, pp. 275–290.
- Hilberts, A.G.J., van Loon, E.E., Troch, P.A., Paniconi, C., 2004. The hillslope-storage Boussinesq model for non-constant bedrock slopes. *J. Hydrol.* 291, 160–173.
- Jakeman, A.J., Hornberger, G.M., 1993. How much complexity is warranted in a rainfall-runoff model. *Water Resour. Res.* 29 (8), 2637–2649.
- Jakeman, A.J., Littlewood, I.G., Whitehead, P.G., 1990. Computation of the instantaneous unit hydrograph and identifiable component flows with application to two small upland catchments. *J. Hydrol.* 117, 275–300.
- Jones, B.E., 1916. A method for correcting river discharge for a changing stage. *US Geological Survey Water Supply Paper No. 375-E*, USGS, pp. 117–130.
- Lam, L., Fredlund, D.G., Barbour, S.L., 1987. Transient seepage model for saturated unsaturated soil systems: a geotechnical engineering approach. *Can. Geotechnol. J.* 24, 565–580.
- Meditch, J.S., 1969. *Stochastic Optimal Linear Estimation and Control*. McGraw-Hill, New York.
- Nathan, R.J., McMahon, T.A., 1990. Evaluation of automated techniques for base flow and recession analysis. *Water Resour. Res.* 26 (7), 1465–1473.
- Paniconi, C., Troch, P.A., van Loon, E.E., Hilberts, A.G., 2003. Hillslope-storage Boussinesq model for subsurface flow and variable source areas along complex hillslopes: 2. Intercomparison with a three-dimensional Richards equation model. *Water Resour. Res.* 39 (11), art. # 1317.
- Parlange, J.-Y., Stagnitti, F., Heilig, A., Szilagyi, J., Parlange, M.B., Steenhuis, T.S., Hogarth, W.L., Barry, D.A., Li, L., 2001. Sudden drainage and drawdown of a horizontal aquifer. *Water Resour. Res.* 37 (8), 2097–2101.
- Pauwels, V.R.N., Verhoest, N.E.C., de Troch, F.P., 2002. A metahillslope model based on an analytical solution to a linearized Boussinesq equation for temporally variable recharge rates. *Water Resour. Res.* 38 (12), art. # 1297.
- Rice, K.C., Hornberger, G.M., 1998. Comparison of hydrochemical tracers to estimate source contributions to peak flow in a small, forested, headwater catchment. *Water Resour. Res.* 34 (7), 1755–1766.
- Robson, A., Beven, K., Neal, C., 1992. Towards identifying sources of subsurface flow: a comparison of components identified by a physically based runoff model and those determined by chemical mixing techniques. *Hydrol. Process.* 6, 199–214.
- Sklash, M.G., Farvolden, R.N., 1979. The role of groundwater in storm runoff. *J. Hydrol.* 43, 45–65.
- Szilagyi, J., 2003a. Sensitivity analysis of aquifer parameter estimations based on the Laplace equation with linearized boundary conditions. *Water Resour. Res.* 39 (6), art. #1156.
- Szilagyi, J., 2003b. State-space discretization of the Kalinin–Milyukov–Nash cascade in a sample-data system framework for streamflow forecasting. *J. Hydrol. Eng.* 8 (6), 339–347.
- Szilagyi, J., 2004a. Accounting for stream–aquifer interactions in the state-space discretization of the Kalinin–Milyukov–Nash cascade for streamflow forecasting. *J. Hydrol. Eng.* 9 (2), 135–143.
- Szilagyi, J., 2004b. Heuristic continuous base flow separation. *J. Hydrol. Eng.* 9 (4), 311–318.
- Szilagyi, J., Parlange, M.B., 1998. Baseflow separation based on analytical solutions of the Boussinesq equation. *J. Hydrol.* 204, 251–260.
- Szilagyi, J., Vorosmarty, C.J., 1997. Modeling unconfined aquifer level reductions in the area between the Danube and Tisza rivers in Hungary. *J. Hydrol. Hydromech.* 45 (5), 328–347.
- Szilagyi, J., Parlange, M.B., Albertson, J.D., 1998. Recession flow analysis for aquifer parameter determination. *Water Resour. Res.* 34 (7), 1851–1857.
- Szilagyi, J., Harvey, F.E., Ayers, J.F., 2003. Regional estimation of base recharge to ground water using water balance and a baseflow index. *Ground Water* 41 (4), 504–513.
- Szollósi-Nagy, A., 1982. The discretization of the continuous linear cascade by means of state-space analysis. *J. Hydrol.* 58, 223–236.
- Szollósi-Nagy, A., 1987. Input detection by the Discrete Linear Cascade Model. *J. Hydrol.* 89, 353–370.
- Szollósi-Nagy, A., 1989. A Mederbeli Lefolyas Real-Time Elorejelzese Dinamikus Strukturális-Sztochasztikus Modellekkkel (Real-Time Streamflow Forecasting with Dynamic Stochastic-System Models, in Hungarian), VITUKI Monographs, Budapest.
- Tallaksen, L.M., 1995. A review of baseflow recession analysis. *J. Hydrol.* 165, 349–370.
- Troch, P.A., de Troch, F.P., Brutsaert, W., 1993. Effective water table depth to describe initial conditions prior to storm rainfall in humid regions. *Water Resour. Res.* 29 (2), 427–434.
- Troch, P.A., Paniconi, C., van Loon, E.E., 2003. Hillslope-storage Boussinesq model for subsurface flow and variable source areas along complex hillslopes: 1. Formulation and characteristic response. *Water Resour. Res.* 39 (11), art. #1316.

- Troch, P.A., van Loon, A.H., Hilberts, A.G.J., 2004. Analytical solution of the linearized hillslope-storage Boussinesq equation from exponential hillslope width functions. *Water Resour. Res.* 40 (8), art. #W08601.
- Young, P., 2001. Data-based mechanistic modelling and validation of rainfall-flow processes. In: Anderson, M.G., Bates, P.D. (Eds.), *Model Validation: Perspectives in Hydrological Science*. Wiley, New York, pp. 117–161.